



Published in final edited form as:

Nat Neurosci. 2018 March ; 21(3): 324–328. doi:10.1038/s41593-018-0074-8.

Mrgprs on vagal sensory neurons contribute to bronchoconstriction and airway hyperresponsiveness

Liang Han^{1,6,*}, Nathachit Limjunyawong^{1,*}, Fei Ru⁴, Zhe Li¹, Olivia J. Hall², Haley Steele⁶, Yuyan Zhu⁶, Julie Wilson⁶, Wayne Mitzner³, Marian Kollarik⁴, Bradley J Undem⁴, Brendan J Canning⁴, and Xinzhong Dong^{1,5}

¹The Solomon H. Snyder Department of Neuroscience, Center for Sensory Biology, School of Medicine

²W. Harry Feinstone Department of Molecular Microbiology and Immunology, Bloomberg School of Public Health

³Department of Environmental Health Sciences, Bloomberg School of Public Health

⁴Department of Medicine, Division of Allergy and Clinical Immunology, School of Medicine

⁵Howard Hughes Medical Institute, Johns Hopkins University, Baltimore, Maryland, USA

⁶School of Biological Sciences, Georgia Institute of Technology, Atlanta, Georgia, USA

Abstract

Asthma, accompanied by lung inflammation, bronchoconstriction, and airway hyperresponsiveness, is a significant public health burden. Here we report that G protein-coupled receptor Mrgprs are expressed in a subset of vagal sensory neurons innervating the airway and mediates cholinergic bronchoconstriction and airway hyperresponsiveness. These findings provide novel insights into the neural mechanisms underlying the pathogenesis of asthma.

The lung is densely innervated by sensory nerves, most of which are derived from the vagal sensory neurons¹. Emerging evidence suggest that sensory nerves in the airway play an important role in the pathogenesis of asthma^{2–5}. MrgprC11, a previously identified itch

Users may view, print, copy, and download text and data-mine the content in such documents, for the purposes of academic research, subject always to the full Conditions of use: http://www.nature.com/authors/editorial_policies/license.html#terms

Correspondence should be addressed to X.D. (xdong2@jhmi.edu) and L.H. (liang.han@biology.gatech.edu).

*These authors contributed equally to this work

Data availability statement: The authors declare that all data generated or analyzed during this study are included within the article and its Supplementary Information files.

Author contributions:

L.H. designed and performed all experiments except where noted. N.L. and L.H. designed and performed all the airway mechanics and IAV infection experiments. F.R. performed the *ex vivo* vagal ganglia GCaMP imaging and RT-PCR of guinea pig airway-innervating vagal sensory neurons. Z.L. performed electrophysiological recording of vagal sensory neurons. O.L. assisted with the IAV infection experiments. H.S. and J.W. performed immunostaining and calcium imaging with HEK293 cells. Y.Z. performed vagal sensory neurons calcium imaging. W.M. supervised the airway mechanics experiments. M.K supervised the *ex vivo* vagal ganglia GCaMP imaging and RT-PCR of guinea pig airway-innervating vagal sensory neurons. B.U. supervised the plethysmography experiments. B.C. conceived and supervised the plethysmography and airway mechanics experiments. X.D. conceived and supervised the project. The manuscript was written by L.H. and X.D. and edited by N.L., W.M., B.U., and B.C.

Competing interests: The authors declare no competing financial interests.

receptor, is expressed in dorsal root ganglion (DRG) sensory neurons innervating the skin and mediates non-histaminergic itch^{6,7}. We found that MrgprC11 is specifically expressed in vagal ganglia besides DRG (Supplementary Fig. 1a). Vagal ganglia consist of two different ganglia, termed nodose and jugular ganglia, with distinct embryonic origins: nodose neurons are derived from the epibranchial placode, while jugular neurons are derived from the neural crest⁸. Using *Wnt1-Cre;R26-IsI-LacZ* mice, in which all the neural crest derived neurons are expressing LacZ, we found that MrgprC11 is selectively expressed in jugular sensory neurons, but not in nodose sensory neurons (Fig. 1a–c, Supplementary Fig. 1c–e and Supplementary Fig. 2). Intriguingly, hMrgprX1, the functional orthologous of MrgprC11, is also selectively expressed in jugular ganglion (Supplementary Fig. 1b).

MrgprC11 immunoreactivity was detected in 6.15% (84/1365) of jugular sensory neurons and in 2.00% (84/4190) of total vagal sensory neurons. MrgprC11⁺ jugular sensory neurons were of small diameter (average $200.27 \pm 9.24 \mu\text{m}^2$), positive for nociceptor marker TRPV1 (Fig. 1d–f), and negative for myelinated neuron marker neurofilament 200kD (Supplementary Fig. 3). We performed retrograde tracing to determine whether MrgprC11⁺ jugular sensory neurons innervate the airway. We observed a total of 750 airway-innervating vagal sensory neurons labeled by retrograde tracer CTB-488 (cholera toxin b subunit conjugated with Alexa 488), and 64 of them were positive for MrgprC11 (Fig. 1g–i), demonstrating that MrgprC11⁺ jugular neurons innervate the airway. However, among the 201 airway-innervating DRG neurons, none of them was positive for MrgprC11 (Fig. 1j–l). Therefore, we concluded that MrgprC11⁺ primary sensory neurons in different sensory ganglia exhibit different peripheral innervation patterns: MrgprC11⁺ jugular sensory neurons innervate the airway, whereas MrgprC11⁺ DRG sensory neurons innervate the skin (Fig. 1m)^{7,9}. These results allow us to attribute the physiological responses in the airway induced by the activation of MrgprC11 to jugular sensory neurons in the following experiments.

Bam8-22, a specific peptide agonist for MrgprC11⁷, can effectively excite MrgprC11⁺ jugular sensory neurons in both calcium imaging assay and whole-cell patch clamp recording (Supplementary Fig. 4a–d). The vagal sensory neurons isolated from *Mrgpr-cluster*^{-/-} mice, in which 12 *Mrgpr* coding sequences including *MrgprC11* were deleted⁷, failed to respond to Bam8-22 (Supplementary Fig. 4a). Among the 12 mouse Mrgprs, MrgprC11 is the only receptor that can respond to Bam8-22 in a heterologous system (Supplementary Fig. 5a–b) and mediate Bam8-22-induced responses in the vagal sensory neurons (Supplementary Fig. 4e–f). To determine whether Bam8-22 can activate airway-innervating vagal sensory neurons, we performed the *ex vivo* GCaMP imaging of vagal ganglia (Supplementary Fig. 6) using *Pirt-Cre; R26-GCaMP6* mice, in which pan-sensory neuron *Pirt* promoter drives the expression of GCaMP6 in >95% of sensory neurons¹⁰. Administration of Bam8-22 onto the airway induced robust Ca²⁺ increase in 2.67% (33/1237, 10 mice) of vagal sensory neurons (Supplementary Fig. 6b–c), suggesting that Bam8-22 activated a subset of jugular sensory neurons innervating the airway.

To elucidate the function of MrgprC11⁺ jugular sensory nerves in the airway, we performed head-out body-plethysmography. Aspiration of Bam8-22 into the airway evoked a change in the respiratory pattern characterized by an increase in the amplitude of the respiratory waveform and a slight but significant increase in the respiratory rate (Fig. 1n–p and

Supplementary Fig. 7a–c). In contrast, Bam8-22 did not induce any change in respiration in *Mrgpr-cluster*^{-/-} mice (Fig. 1o, p, Supplementary Fig. 7a–c). The Bam8-22-induced respiratory effect was similar to that observed upon the administration of methacholine, a bronchoconstrictor acting on muscarinic acetylcholine receptor (mAChR) in airway smooth muscle (Fig. 1n, q, r and Supplementary Fig. 7d–e). Both Bam8-22- and methacholine-induced respiratory effects were blocked by ipratropium bromide, a mAChR blocker (Fig. 1q–r, Supplementary Fig. 7d–e). Administration of capsaicin to activate TRPV1⁺ vagal sensory neurons induced a different respiratory response characterized by a cessation in breathing that persisted for an average of 5.66 ± 0.81 s, followed by a secondary phase with diminished frequency and prolonged braking after each breath (Fig. 1n). This is a prototypic response induced by the administration of respiratory sensory irritants such as cigarette smoke and cinnamaldehyde into the respiratory tract^{11–14}. It is interesting that although MrgprC11⁺ jugular sensory neurons are expressing TRPV1, the respiratory reflexes evoked by Bam8-22 and capsaicin are quite different. These results suggest that activation of a few afferents by Bam8-22 versus a large population by capsaicin can produce nonlinear effects in lung responses.

The similarity between Bam8-22 and methacholine-induced respiratory responses led us to the hypothesis that Bam8-22 may induce bronchoconstriction, which we tested by measuring airway mechanics. Retro-orbital intravenous injection of Bam8-22 significantly increased lung resistance (R_L) in WT mice but not in *Mrgpr-cluster*^{-/-} mice (Fig. 2b and Supplementary Fig. 8a–b), demonstrating that Bam8-22 induces bronchoconstriction. Stimulation of a subset of vagal sensory neurons caused release of acetylcholine from parasympathetic nerve fibers, which in turn acts on the mAChR in airway smooth muscle to induce bronchoconstriction (Fig. 2a)¹⁵. This parasympathetic cholinergic pathway is the major neural mechanism controlling bronchoconstriction in the lung¹⁵. The Bam8-22-induced increase in lung resistance was completely blocked by ipratropium bromide (Fig. 2c) and vagotomy surgery (Fig. 2d), which severs the vagus nerve, demonstrating that Bam8-22 induced cholinergic bronchoconstriction. Bam8-22-induced bronchoconstriction was not affected by the deletion of TRPA1 or TRPV1 (Supplementary Fig. 8c). Bam8-22 did not cause tracheal smooth muscle contraction (Fig. 2e), ruling out the possibility that Bam8-22 directly stimulates airway smooth muscle. Taken together, these data suggest that Bam8-22 activates MrgprC11⁺ jugular sensory neurons that in turn stimulates the parasympathetic system and induces cholinergic bronchoconstriction.

We also observed similar Bam8-22-induced effects in guinea pigs, another animal species that is frequently used to study respiratory reflex and to model respiratory diseases. *gpMrgprx1* (XM_003462608), the predicted *Mrgprc11* ortholog, is expressed in airway-innervating jugular and nodose neurons (Supplementary Fig. 9a–b). Bam8-22 activated guinea pig vagal sensory neurons in a *gpMrgprx1*-dependent way (Supplementary Fig. 9c–e). Excitingly, intravenous injection of Bam8-22 in guinea pigs induces robust bronchoconstriction (Fig. 2f, Supplementary Fig. 9f). However, whether Bam8-22 also activates vagal-cholinergic reflex to induce bronchoconstriction in guinea pigs, as it does in mice, requires further investigations.

Anaphylaxis is an acute, potentially life-threatening allergic reaction mediated by mast cell activation. Anaphylactic symptoms in the respiratory system include coughing, airway swelling, and bronchoconstriction¹⁶. Retro-orbital injection of OVA resulted in a pronounced increase in lung resistance in OVA-sensitized WT mice (Fig. 3a). This effect was significantly inhibited in sensitized *Mrgpr-cluster*^{-/-} mice (Fig. 3a and Supplementary Fig. 8d), suggesting that Mrgprs mediate anaphylactic bronchoconstriction. Anaphylactic bronchoconstriction is evoked mainly by mast cell mediators acting on both airway smooth muscle and sensory nerves¹⁷. Interestingly, neuropeptide FF (NPFF), an MrgprC11 agonist that can be released by activated mouse bone marrow-derived mast cells¹⁸, also induced bronchoconstriction (Fig. 3b, Supplementary Fig. 8e). Additional studies are required to determine whether Mrgprs play a role in the sensitization of mast cells, their activation, or both.

Influenza virus infection causes characteristic effects within the respiratory tract, including airway inflammation and airway hyperresponsiveness. It is a major risk factor for exacerbation of asthma and causes significant morbidity and mortality annually¹⁹. We infected WT and *Mrgpr-cluster*^{-/-} mice with Influenza A virus (IAV) to examine whether sensory nerves contribute to IAV-induced respiratory symptoms. Both WT and *Mrgpr-cluster*^{-/-} mice displayed robust immune responses after inoculation (Fig. 3d, Supplementary Fig. 10a–b). However, we observed significantly lower IAV-induced airway hyperresponsiveness in *Mrgpr-cluster*^{-/-} mice compared to WT mice (Fig 3c), demonstrating that Mrgprs are required for IAV-induced airway hyperresponsiveness. The deletion of Mrgpr genes did not affect the airway hyperresponsiveness in a house dust mite-induced allergic asthma model (Supplementary Fig. 11). These data suggest that distinct mechanisms exist for the development of airway hyperresponsiveness under different pathological conditions.

We next asked whether direct stimulation of MrgprC11⁺ jugular sensory neurons could induce airway hyperresponsiveness in the absence of lung inflammation. We pretreated WT and *Mrgpr-cluster*^{-/-} mice with Bam8-22 to activate MrgprC11⁺ jugular sensory neurons. 5 min after Bam8-22 treatment, when the Rrs has returned to their baseline level, the airway responsiveness to MCh were measured in WT and *Mrgpr-cluster*^{-/-} mice. We found that pretreatment with Bam8-22 caused a remarkable increase in airway responsiveness in WT mice, but not in *Mrgpr-cluster*^{-/-} mice (Fig. 3e). As expected, the enhanced airway sensitivity was abolished by vagotomy in WT mice (Fig. 3f). These data demonstrated that activation of MrgprC11⁺ jugular sensory neurons can potentiate airway responsiveness in the absence of inflammation. Airway responsiveness to MCh is the result of both direct action on airway smooth muscle and muscle contraction-induced vagal reflex^{15,20}. Our data, which is consistent with previous studies^{3,4}, supports the hypothesis that the activation of vagal C-fiber by Bam8-22 may lead to the sensitization of the vagal afferent-brainstem-parasympathetic reflex pathway and enhance airway responsiveness. Full length of the DNA gel images are presented in Supplementary Fig. 12.

In summary, we demonstrated that MrgprC11⁺ jugular sensory neurons, constituting only 2% of vagal sensory neurons, mediate cholinergic bronchoconstriction and play a role in the development of airway hyperresponsiveness in mice. Therapeutic approaches targeting this

small population will avoid the possible side effects of antagonizing all vagal nociceptors, which play important roles in maintaining the physiological functions of multiple inner organs. Future studies investigating the endogenous agonists of MrgprC11 in the lung, the peripheral/central axonal projections of MrgprC11⁺ neurons, and the neural circuit in which these neurons reside will further reveal the neural mechanisms of respiratory diseases. The *Mrgpr-cluster*^{-/-} mice exhibited decreased anaphylactic bronchoconstriction and reduced airway hyperresponsiveness after influenza virus infection. Since 12 Mrgpr genes were deleted in the *Mrgpr-cluster*^{-/-} mice, the phenotypes observed may not be mediated solely by MrgprC11. Whether the other Mrgpr genes are involved in the tested models requires further investigation.

Online Methods

Animals

All experiments were performed with approval from the Johns Hopkins University Animal Use and Care Committee and the Georgia Institute of Technology Animal Use and Care Committee. The generation of *Mrgpr-cluster*^{-/-} mice was described previously⁷ and they had been backcrossed to C57Bl/6J mice for at least ten generations. Wnt1-Cre and ROSA26-lsl-LacZ mouse lines were purchased from Jackson Laboratory. Pirt-Cre line was generated in Dong's Laboratory. ROSA26-lsl-GCaMP6 line was kindly provided by Dwight Bergles at Johns Hopkins University. 3 weeks old male animals were used for Ca²⁺ imaging assay. 2-3 months old males were used for all other experiments. 200-250 grams male Hartley Guinea pigs were purchased from Charles River. All the animals were housed in the vivarium with a 12-hr-light/dark cycle, and all the behavioral tests were performed from 9 a.m. to 1 p.m. in the light cycle. The housing group was 5 at maximum for mice and 2 at maximum for guinea pigs.

Retrograde tracing of sensory neurons innervating the airway

Mice were anesthetized with pentobarbital (70 mg/kg) and the ventral upper tracheal region was exposed and pierced with a microinjecting needle attached to a Hamilton syringe. Retrograde tracer CTB-488 (cholera toxin b subunit conjugated with Alexa 488, 20 µl, 1 mg/ml) was directly injected into the tracheal lumen. Vagal ganglia and DRG were collected 7 days after the injection to perform immunohistochemical analysis. Male Hartley guinea pigs (250 to 300 g) were anesthetized with ketamine/xylazine (50 mg/kg ketamine and 2.5 mg/kg xylazine). DiI (0.2%, 200 µl; in 10% DMSO and 90% saline, invitrogen D282) was delivered into the airway as previously described²¹. Briefly, a tracheotomy was performed and the caudal part of the trachea was exposed. DiI was injected into the lumen of the trachea with a syringe needle.

RT-PCR

Total RNA was extracted from various tissues using Trizol reagent (Invitrogen) according to the manufacturer's instructions. Mouse tissues were collected from 2-3 months old C57Bl/6 male mice. Reverse transcription was carried out using the Superscript III first-strand synthesis system (Invitrogen). PCR conditions for mouse Mrgpr genes, *hMrgprX1*, *hTRPV1*

and *hGAPDH*: 95 °C for 3 min, 40 cycles of 30 s at 95 °C, 30 s at 55 °C and 60 s at 72 °C. All the PCR results were confirmed by DNA sequencing.

RT-PCR with human tissues

Human jugular and nodose ganglia were purchased from Tissue for Research (Tissue4Research.com). The results were repeated 5 times with vagal ganglia collected from 5 different donors. Characteristics and medical history of patients from whom the tissues were collected are shown in the table below. The procedure was approved by Georgia Tech Biological Materials Safeguards Committee. Human lung total RNA was purchased from OriGene.

Patient #	Age	Sex	Race	Height/Weight	Cause of death
1	75	F	White	5'5"/170 lbs	Ovarian Cancer
2	60	M	White	5'10"/175lbs	Melanoma
3	44	F	White	5'3"/120 lbs	Colon cancer
4	84	F	White	5'3"/112 lbs	End stage COPD
5	72	M	White	5'7"/140 lbs	Pancreatic cancer

RT-PCR with guinea pig airway-innervating neurons

Dissociated jugular and nodose ganglia neurons were cultured on coverslips 14 days after the DiI injection. Individual DiI labelled cells were identified by fluorescent microscope and harvested by glass-pipette into PCR tubes that contained 1 µl of RNase inhibitor (Invitrogen). The cells were immediately placed on dry ice after collection. About 25 cells were pooled into each PCR tube. Cells were processed using Superscript III CellsDirect cDNA Synthesis Kit (Invitrogen) according to the manufacturer's instruction to generate first strand cDNA. All the primers for *gpMrgprX1*, *gpTRPV1* and *gpACTB* are intron-spanning. PCR conditions: 95 °C for 5 min, 50 cycles of 30 s at 95 °C, 30 s at 55 °C and 45 s at 72 °C. All the PCR results were confirmed by DNA sequencing.

The sequence of the primers used were as follows

Gene	Primer sequence (5' – 3')
<i>MrgprA1-F</i>	ATCCAGCAAGAGGAATGGGG
<i>MrgprA1-R</i>	TGTGACCTAGGAGGAAGAAGAAG
<i>MrgprA2-F</i>	CCTCCTACACAAGCCAGCAA
<i>MrgprA2-R</i>	AAGCAC AAGTGAAAGATGATGCT
<i>MrgprA3-F</i>	GCTACATCCAGCAAGAGGAATG
<i>MrgprA3-R</i>	GCAAAAATTCCTTTGGGTAGGGT
<i>MrgprA4-F</i>	CCTGTGTGCTGTGATCTGGT
<i>MrgprA4-R</i>	TCACGGTTAATCCAGGGCAC
<i>MrgprA10-F</i>	CAGTGGTCCACCATCTCCAA
<i>MrgprA10-R</i>	ACAGGCAAGAGAGTCATGGTT
<i>MrgprA12-F</i>	TCAGGGATCGGGTGAAGCAC

<i>MrgprA12-R</i>	GAGCATTTGAAGGTGTTGTTGGA
<i>MrgprA14-F</i>	GGTGGCCCTGTGTTCTTC
<i>MrgprA14-R</i>	TATTGCCAGTCAGTAAGCTGAG
<i>MrgprA16-F</i>	GCCCTCTGGTTCCCACTACT
<i>MrgprA16-R</i>	GTTTTGGACCACTGAGGCATT
<i>MrgprA19-F</i>	CAGGACCCAGATCACGACAC
<i>MrgprA19-R</i>	TCCTGGGCTTCCGATTTAC
<i>MrgprB4-F</i>	TCTGGCTGGTGCTGATTCTT
<i>MrgprB4-R</i>	ACCACGAGGCTCAACAATAGA
<i>MrgprB5-F</i>	CTGTGGTTTCTTCTGTGTCCA
<i>MrgprB5-R</i>	TTTCCAGTTCCTCCAGACCTT
<i>MrgprC11-F</i>	AGCATCCACAACCCAGAAG
<i>MrgprC11-R</i>	TGGAGTGCAGTTGGGATGAC
<i>mACTB-F</i>	CGTCGACAACGGCTCCGGCATG
<i>mACTB-R</i>	CCACCATCACACCCTGGTGCCTAGG
<i>gpMrgprX1-F</i>	GCTGCCACTCATCCTGAGAA
<i>gpMrgprX1-R</i>	ATCCACGCTCACAACCCTT
<i>gpTRPV1-F</i>	GGCCAATGGGGACTTCTTCA
<i>gpTRPV1-R</i>	GAGTCCCTGGCACTGATGTC
<i>gpACTB-F</i>	TGCTGCGTTACACCTTTCT
<i>gpACTB-R</i>	GCTCCAACCAACTGCTGTCA
<i>hMrgprX1-F</i>	AGCGGCCGCCTTATATATTCC
<i>hMrgprX1-R</i>	AGCTCAGGCCTGCAAAGTAG
<i>hTRPV1-F</i>	GTGCTGTACTTCAGCCACCT
<i>hTRPV1-R</i>	TGAAACGGCACAGGTCTCTC
<i>hGAPDH-F</i>	TGGTCTCCTCTGACTTCAACAGCG
<i>hGAPDH-R</i>	AGGGGTCTACATGGCAACTGTGAG

Immunostaining

Adult mice (8-12 weeks old) were anesthetized with pentobarbital and perfused with 4% paraformaldehyde in PBS. Vagal ganglia and dorsal root ganglia (DRG) were dissected from the perfused mice for immunostaining. The tissues were postfixed, cryoprotected in 30% sucrose, and sectioned with a cryostat. The primary antibodies used: rabbit polyclonal anti-MrgprC11 (made by Proteintech Group, Inc.), chicken anti-LacZ (Abcam, ab9361), guinea-pig anti-TRPV1 (Chemico, ab5566), chicken anti-NF-200 (Aves, NFH), rat anti-subP (Millipore, MAB356), Tubulin β 3 (Covance, PRB-435P). All the secondary antibodies were purchased from Invitrogen: Donkey anti-Rabbit IgG-Alexa Fluor 555 (A-31572), Goat anti-Chicken IgY-Alexa Fluor 488 (A-11039), Goat anti-Guinea Pig IgG-Alexa Fluor 488 (A-11073), Donkey anti-Rat IgG Alexa Fluor® 488 (A-21208), Goat anti-mouse IgG-Alexa Fluor 488 (A11001). To detect IB4 binding, sections were incubated with 1:200 diluted IB4-Alexa 488 (I-21411, Invitrogen) during secondary antibody incubations. MrgprC11 antibody was validated with *Mrgpr-cluster*^{-/-} mice (Supplementary Fig. 2). Validation data for other antibodies are available from the commercial providers.

Calcium imaging

Calcium imaging was performed as previously described⁹. Briefly, cells (HEK293 cells, vagal sensory neurons from 3-4 weeks old mice, or vagal sensory neurons from 200-250 grams guinea pigs) were cultured on glass coverslips. Cells were loaded with fura 2-acetomethoxy ester (Molecular Probes) for 30 min in the dark at room temperature. After washing, cells were imaged at 340 and 380 nm excitation to detect intracellular free calcium and 20% increase in F340/F380 was set as threshold. Average fluorescence ratios (F340/F380) were calculated from 20 cells and all the population data are presented as mean \pm s.e.m.

Whole-cell current-clamp recordings of vagal sensory neurons

Bam8-22-responding vagal sensory neurons were first identified by calcium imaging before they were patched for current clamp recording. Patch pipettes had resistances of 2–4 M Ω . Action potential measurements were performed with an Axon 700B amplifier and the pCLAMP 9.2 software package (Axon Instruments). Neurons were perfused with 2 μ M Bam8-22 for 20s. All experiments were performed at room temperature.

Ex vivo vagal ganglia GCaMP imaging

A modification of the method described previously²² was used for the dissection and tissue preparation. Briefly, mice were sacrificed by CO₂ inhalation and exsanguination. The blood from the pulmonary circulation was mostly washed out by in situ perfusion with 20 ml of Krebs-bicarbonate solution (KBS) containing (in mM): 118 NaCl, 5.4 KCl, 1 NaH₂PO₄, 1.2 MgSO₄, 1.9 CaCl₂, 25 NaHCO₃, 11.1 dextrose. The trachea and the lung with intact vagus nerves and vagal ganglia were dissected and placed in a two-compartment tissue chamber (Supplementary Figure 6a). The lung was pinned in one compartment (airway chamber) to receive chemical stimuli. The left vagal ganglia (VG chamber) were pinned in a second compartment for multiphoton imaging. Both compartments were perfused with 37 °C KBS. There is no fluid exchange between the two compartments. The trachea was cannulated with PE tubing to allow the delivery of chemicals onto the airway. The lungs were punctured with a 27-gauge needle (1–2 mm deep, 2–8 per lobe) to allow perfusing KBS to exit the tissue. The surface of the rostral vagal ganglia was imaged by a multiphoton microscope (Scientifica) with a 20 \times water immersion lens.

Head-out body-plethysmography

Head-out body-plethysmography was performed with anesthetized and spontaneously breathing mice. Mice were anesthetized with urethane and tracheostomy was performed to allow the aspiration of chemicals (2 μ l, 1 mM capsaicine, 1 mM MCh, 5 mM Bam8-22) directly into the trachea through the cannula. Delivery of the chemicals directly into the trachea allows us to avoid interference from the upper respiratory tract, which is mainly innervated by trigeminal sensory neurons. The body of the animal was kept in a chamber and the respiratory effort was monitored digitally using a Biopac data acquisition system. Respiratory rate and the amplitude of the respiratory waveform were analyzed offline with AcqKnowledge software.

Airway mechanics

Anesthetized (pentobarbital, 70 mg/kg) animals were tracheotomized, attached to a Flexivent pulmonary mechanics analyzer (SCIREQ), and paralyzed with succinylcholine (2 mg/kg). Anesthetized mice were ventilated at a tidal volume of 9 mL/kg, at a frequency of 150 bpm. Anesthetized guinea pigs were ventilated at a tidal volume of 8 mL/kg, at a frequency of 90 bpm. Positive end-expiratory pressure was set at 3 cm H₂O. We assessed the airway responsiveness using a single-compartment model to measure the total lung resistance (R_L), a dynamic variable that is largely dependent on the resistance to air flow through the airways and is sensitive to airway smooth muscle contraction. Bam8-22 (50 μ l, 10 mg/ml for mice, 400 μ l, 20 mg/ml for guinea pigs), NPFF (50 μ l, 10 mg/ml), and MCh (50 μ l, 30 μ g/ml) were administered by retro-orbital IV injection. Airway hyperresponsiveness was determined in response to aerosolized methacholine challenges (0, 1, 3, 10, and 30 mg/ml). The nebulizer was on for 10 seconds to deliver each dose of MCh.

Organ bath studies

Organ bath studies were performed as previously described²³. Briefly, whole tracheas were dissected out from sacrificed mice and placed in oxygenated Krebs-bicarbonate solution containing (in mM): 118 NaCl, 5.4 KCl, 1 NaH₂PO₄, 1.2 MgSO₄, 1.9 CaCl₂, 25 NaHCO₃, 11.1 dextrose. Tracheas were cleaned of connective tissue and tracheal rings (whole or laterally divided in half), were suspended between two tungsten stirrups in 10 ml organ chambers filled with Krebs solution that was warmed to 37 °C and bubbled with 95% O₂–5% CO₂ to maintain a pH of 7.4. One stirrup was connected to a strain gauge (model FT03; Grass Instruments, Quincy, MA, USA), and tension was recorded on a Grass Model 7 polygraph (Grass Instruments). Preparations were stretched to a resting tension of 0.2 g, and washed with fresh Krebs buffer at 15 min intervals during a 60-min equilibration period. After equilibration, tracheas were challenged with either Bam8-22 (10 μ M) or electrical field stimulation (12V, 8HZ, 0.5ms, 10s/100s). At the end of each experiment, all tracheas were maximally contracted with carbamylcholine (1mM). The results are expressed as a percentage of maximum contraction.

IAV infection-induced lung inflammation

Mouse adapted influenza A/California/4/2009 H1N1 was a kind gift from Dr. Sabra Klein in the Department of Molecular Microbiology and Immunology at Johns Hopkins University School of Public Health. 8-12-week old mice were anesthetized with ketamine (100 mg/kg) and xylazine (15 mg/kg) and were infected intranasally with 0.4 50% mouse lethal dose (MLD50) of IAV in 30 μ l of DMEM. Mice in the control group were infected with 30ul DMEM medium only. At 5 days post infection, the airway mechanics were examined using the Flexivent system and the bronchoalveolar lavage fluid (BALF) was collected to evaluate lung inflammation. BALF was centrifuged and the cell pellet was resuspended in PBS to perform differential cell counting of leukocytes (macrophages/monocytes, neutrophils, eosinophils, and lymphocytes). The supernatant of BALF was used to examine the levels of TNF- α , IFN- γ , and IL-6 using enzyme immunoassay kits purchased from R&D Systems (Minneapolis, MN) according to individual kit instructions. Lungs were inflated and fixed

with formalin at 30 cm H₂O and lung sections were processed and stained with hematoxylin and eosin.

Mouse model of anaphylaxis

Mice were sensitized with 20 µg of OVA emulsified with 2 mg of Inject Alum Adjuvant in 150 µl PBS by i.p. injection. 21 days after OVA sensitization, mice were anesthetized and challenged with 500ug of OVA in 50 µl of PBS and the airway mechanics were measured using the Flexivent system. The airway resistance increased gradually after the OVA injection, reaching the peak at 50-60 seconds after the injection. To examine the level of OVA-specific IgE, serum of sensitized mice was collected on day 18 (before challenge). The OVA-specific IgE level was determined using the anti-Ovalbumin IgE (mouse) ELISA kit (CaymanChemical, 500840) following the user's instructions.

House dust mite-induced airway allergic inflammation

Mice were sensitized by i.p. injection of 100 µg house dust mite extract in 150 µl PBS on days 1 and 14. Lightly anesthetized mice (isoflurane) were challenged by intranasal instillation of 100 µg house dust mite extract in 20 µl PBS on days 18 and 21. Airway mechanics measurements were performed on day 23.

Data analysis and statistics

Statistical analyses were performed using Prism 7 (GraphPad). We did not use statistical methods to predetermine the sample size. Our sample sizes are comparable to those reported in previous publications. Differences between experimental groups were analyzed with two-tailed unpaired Student's t test. Threshold for significance (α) was set at 0.05. Data are reported as mean \pm s.e.m.. Normality and equality of variance were analyzed with the Shapiro-Wilk normality test and F-test, respectively. When the sample numbers were too small to calculate, distribution was assumed to be normal. The experimenters were blinded to the genotype of the animals. Animals were assigned randomly to the various experimental groups, and data were collected and processed randomly. N numbers were indicated for all the experiments that required statistical analysis. RT-PCR and immunostaining were performed at least three times with three different animals. Retrograde tracings were performed three times using three animals each time. A Life Sciences Reporting Summary is available online.

Supplementary Material

Refer to Web version on PubMed Central for supplementary material.

Acknowledgments

This study was supported by grants from the NIH (NS054791 to X.D., NS087088 to L.H., HL010342 to W.M., HL112919 to B.U., DK110366 to MK, and HL122228 to B.C.) and by the American Asthma Foundation (to X.D.). We thank M. Anderson at Johns Hopkins University Pain Imaging Core for assisting *ex vivo* vagal GCaMP imaging. We thank S. Klein at Johns Hopkins University Department of Molecular Microbiology and Immunology for providing the mouse-adapted influenza A/California/04/2009 H1N1 virus. We thank R. Rabold and L. Zhen for providing technical support for Flexivent experiments.

References

1. Mazzone SB, Canning BJ. Autonomic neural control of the airways. *Handb Clin Neurol*. 2013; 117:215–228. DOI: 10.1016/B978-0-444-53491-0.00018-3 [PubMed: 24095128]
2. Talbot S, et al. Silencing Nociceptor Neurons Reduces Allergic Airway Inflammation. *Neuron*. 2015; 87:341–354. DOI: 10.1016/j.neuron.2015.06.007 [PubMed: 26119026]
3. McAlexander MA, Gavett SH, Kollarik M, Udem BJ. Vagotomy reverses established allergen-induced airway hyperreactivity to methacholine in the mouse. *Respir Physiol Neurobiol*. 2015; 212–214:20–24. DOI: 10.1016/j.resp.2015.03.007
4. Trankner D, Hahne N, Sugino K, Hoon MA, Zuker C. Population of sensory neurons essential for asthmatic hyperreactivity of inflamed airways. *Proc Natl Acad Sci U S A*. 2014; 111:11515–11520. DOI: 10.1073/pnas.1411032111 [PubMed: 25049382]
5. Caceres AI, et al. A sensory neuronal ion channel essential for airway inflammation and hyperreactivity in asthma. *Proc Natl Acad Sci U S A*. 2009; 106:9099–9104. DOI: 10.1073/pnas.09005911106 [PubMed: 19458046]
6. Sikand P, Dong X, LaMotte RH. BAM8-22 peptide produces itch and nociceptive sensations in humans independent of histamine release. *J Neurosci*. 2011; 31:7563–7567. DOI: 10.1523/JNEUROSCI.1192-11.2011 [PubMed: 21593341]
7. Liu Q, et al. Sensory neuron-specific GPCR Mrgprs are itch receptors mediating chloroquine-induced pruritus. *Cell*. 2009; 139:1353–1365. DOI: 10.1016/j.cell.2009.11.034 [PubMed: 20004959]
8. Baker CV, Schlosser G. The evolutionary origin of neural crest and placodes. *J Exp Zool B Mol Dev Evol*. 2005; 304:269–273. DOI: 10.1002/jez.b.21060 [PubMed: 16003767]
9. Han L, et al. A subpopulation of nociceptors specifically linked to itch. *Nat Neurosci*. 2013; 16:174–182. DOI: 10.1038/nn.3289 [PubMed: 23263443]
10. Kim YS, et al. Central terminal sensitization of TRPV1 by descending serotonergic facilitation modulates chronic pain. *Neuron*. 2014; 81:873–887. DOI: 10.1016/j.neuron.2013.12.011 [PubMed: 24462040]
11. Taylor-Clark TE, Kiros F, Carr MJ, McAlexander MA. Transient receptor potential ankyrin 1 mediates toluene diisocyanate-evoked respiratory irritation. *Am J Respir Cell Mol Biol*. 2009; 40:756–762. DOI: 10.1165/rcmb.2008-0292OC [PubMed: 19059884]
12. Nassenstein C, et al. Expression and function of the ion channel TRPA1 in vagal afferent nerves innervating mouse lungs. *J Physiol*. 2008; 586:1595–1604. DOI: 10.1113/jphysiol.2007.148379 [PubMed: 18218683]
13. Ha MA, et al. Menthol attenuates respiratory irritation and elevates blood cotinine in cigarette smoke exposed mice. *PLoS One*. 2015; 10:e0117128. [PubMed: 25679525]
14. Nassenstein C, et al. Pulmonary distribution, regulation, and functional role of Trk receptors in a murine model of asthma. *J Allergy Clin Immunol*. 2006; 118:597–605. DOI: 10.1016/j.jaci.2006.04.052 [PubMed: 16950277]
15. Canning BJ. Reflex regulation of airway smooth muscle tone. *J Appl Physiol* (1985). 2006; 101:971–985. DOI: 10.1152/jappphysiol.00313.2006 [PubMed: 16728519]
16. Nel L, Eren E. Peri-operative anaphylaxis. *Br J Clin Pharmacol*. 2011; 71:647–658. DOI: 10.1111/j.1365-2125.2011.03913.x [PubMed: 21235622]
17. Udem BJ, Taylor-Clark T. Mechanisms underlying the neuronal-based symptoms of allergy. *J Allergy Clin Immunol*. 2014; 133:1521–1534. DOI: 10.1016/j.jaci.2013.11.027 [PubMed: 24433703]
18. Lee MG, et al. Agonists of the MAS-related gene (Mrgs) orphan receptors as novel mediators of mast cell-sensory nerve interactions. *J Immunol*. 2008; 180:2251–2255. [PubMed: 18250432]
19. Lambrecht BN, Hammad H. The immunology of asthma. *Nat Immunol*. 2015; 16:45–56. DOI: 10.1038/ni.3049 [PubMed: 25521684]
20. Udem BJ, Kajekar R, Hunter DD, Myers AC. Neural integration and allergic disease. *J Allergy Clin Immunol*. 2000; 106:S213–220. [PubMed: 11080734]

Methods-only references

21. Kwong K, et al. Voltage-gated sodium channels in nociceptive versus non-nociceptive nodose vagal sensory neurons innervating guinea pig lungs. *J Physiol.* 2008; 586:1321–1336. DOI: 10.1113/jphysiol.2007.146365 [PubMed: 18187475]
22. Undem BJ, et al. Subtypes of vagal afferent C-fibres in guinea-pig lungs. *J Physiol.* 2004; 556:905–917. DOI: 10.1113/jphysiol.2003.060079 [PubMed: 14978204]
23. Weigand LA, Myers AC, Meeker S, Undem BJ. Mast cell-cholinergic nerve interaction in mouse airways. *J Physiol.* 2009; 587:3355–3362. DOI: 10.1113/jphysiol.2009.173054 [PubMed: 19403609]

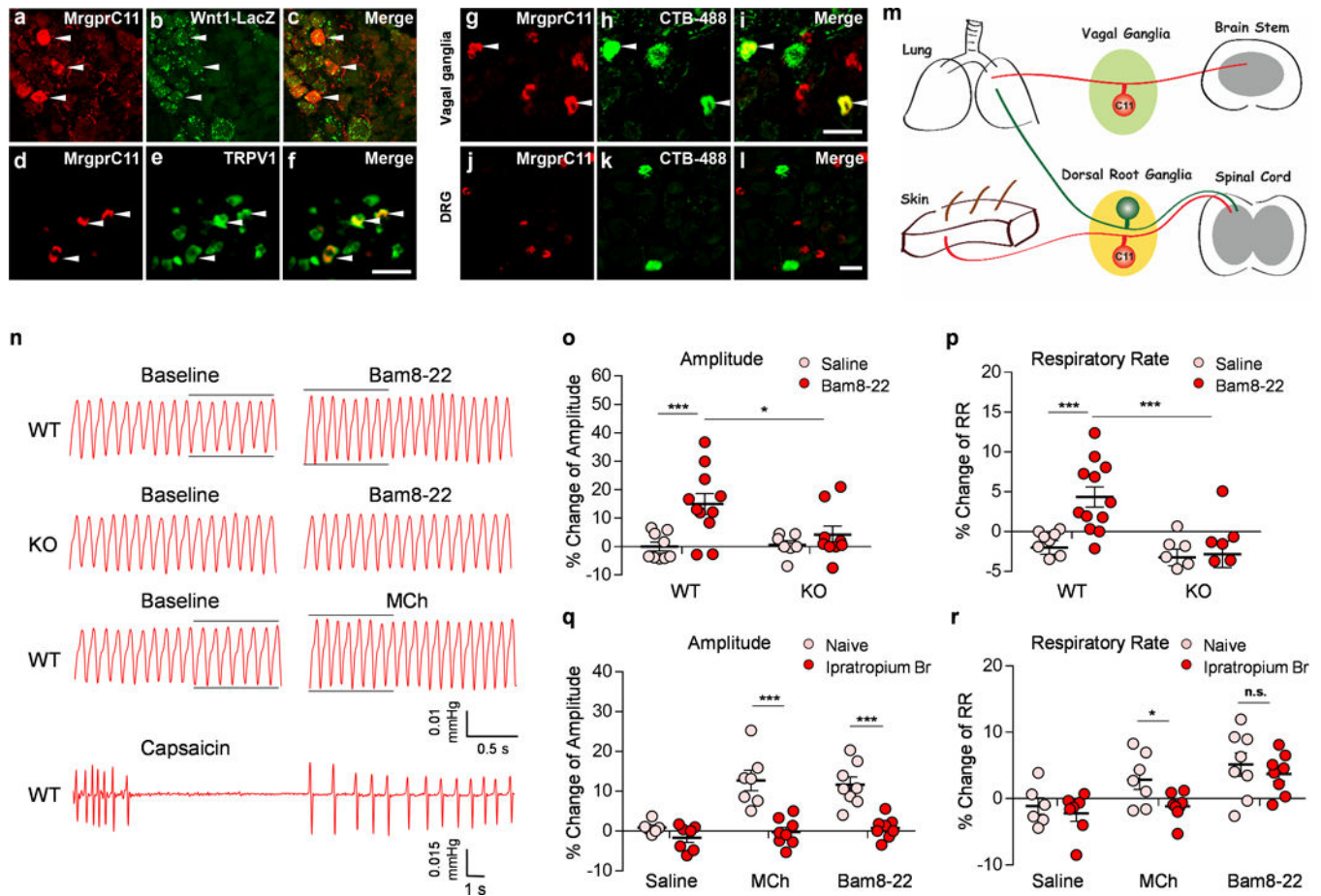


Figure 1. Activation of MrgprC11⁺ sensory nerves in the airway changes the respiratory pattern in mice

(a-c) Sections of vagal ganglia from *Wnt1-Cre; ROSA26^{lacZ}* mice were stained with antibodies against MrgprC11 (red) and LacZ (green). MrgprC11 is only expressed in jugular sensory neurons labeled by lacZ. (d-f) MrgprC11⁺ jugular sensory neurons are positive for nociceptor marker TRPV1. (g-l) Sections of vagal ganglia (g-i) and DRG (j-l) from animals that were injected with retrograde neuronal tracer CTB-488 intratracheally were stained with antibodies against MrgprC11 (red). Airway-innervating neurons were indicated by CTB-488 fluorescence (green). Lower magnification images of DRG sections were presented to show the sparse airway-innervating neurons. Arrowheads mark representative MrgprC11⁺ airway-innervating neurons. (m) Diagram showing the peripheral innervation patterns of MrgprC11⁺ sensory neurons in DRG and vagal ganglia. MrgprC11⁺ jugular sensory neurons innervate the lung, whereas MrgprC11⁺ DRG sensory neurons innervate the skin. (n) Representative traces of pulmonary airflow waveforms from wild-type and *Mrgpr-cluster*^{-/-} mice at baseline and 1 min (peak time) after intratracheal instillation of 2 μ l Bam8-22 (10 mg/ml), MCh (0.2 mg/ml) and capsaicin (0.3 mg/ml). (o-p) Bam8-22 evoked an increase in the amplitude of the respiratory waveform (o) and an increase in the respiratory rate (p) in WT mice, but not in *Mrgpr-cluster*^{-/-} mice. (WT-Saline, n=9; WT-Bam8-22, n=11; KO-Saline, n=7; KO-Bam8-22, n=8; for (o), WT-Saline vs WT-Bam8-22, p=0.0022; WT-Bam8-22 vs KO-Bam8-22, p=0.029; for (p) WT-Saline vs WT-Bam8-22, p=0.0003; WT-

Bam8-22 vs KO-Bam8-22, $p=0.0038$). (q-r) Bam8-22-induced respiratory effect was similar to that observed upon the administration of methacholine, a bronchoconstrictor. Ipratropium bromide, a cholinergic blocker, inhibited the increase of the amplitude of the respiratory waveform induced by Bam8-22 (q). Ipratropium bromide did not inhibit the increase of the respiratory rate induced by Bam8-22 (r). All methacholine-induced respiratory effects were blocked by ipratropium bromide. (Naive-Saline, $n=6$; Ipra-Saline, $n=7$; Naive-MCh, $n=7$; Ipra-MCh, $n=8$; Naive-Bam8-22, $n=8$; Ipra-Bam8-22, $n=8$; for (q), Naive-MCh vs Ipra-MCh; $p=0.0003$; Naive-Bam8-22 vs Ipra-Bam, $p=0.0001$; for (r), Naive-MCh vs Ipra-MCh, $p=0.039$; Naive Bam vs Ipra-Bam, $p=0.509$). All the immunostaining, retrograde tracing, and plethysmograph experiments were repeated independently three times with similar results. Scale bars represent $50 \mu\text{m}$. *** $p < 0.005$, ** $p < 0.01$, * $p < 0.05$, two-tailed unpaired Student's t test. Data are reported as mean \pm s.e.m.

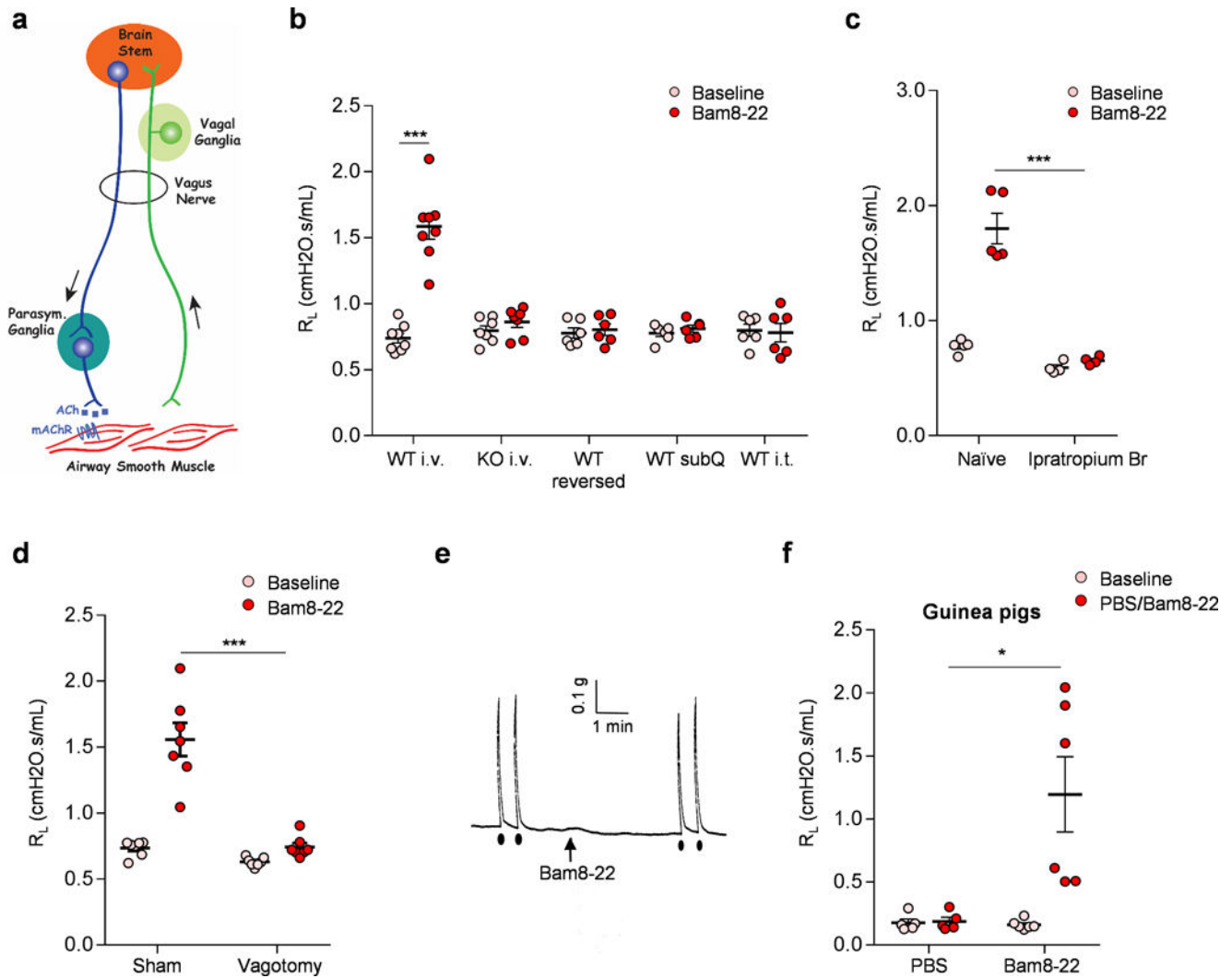


Figure 2. *MrgprC11*⁺ jugular sensory neurons mediate cholinergic bronchoconstriction
 (a) Diagram showing the neural pathway mediating parasympathetic cholinergic bronchoconstriction. (b) Retro-orbital I.V. injection of Bam8-22 induced bronchoconstriction in WT, but not *Mrgpr-cluster*^{-/-} mice. Reversed Bam8-22 peptide did not induce bronchoconstriction. Subcutaneous and intrathecal administration of Bam8-22 to activate the peripheral and central terminals of *MrgprC11*⁺ DRG sensory neurons, respectively, did not induce bronchoconstriction, consistent with the fact that *MrgprC11*⁺ DRG sensory neurons do not innervate the airway. (WT i.v., n=8; KO iv, n=7; WT reversed, n=6; WT subQ, n=6; WT i.t. n=6; WT i.v. Baseline vs Bam8-22, p=5.36E-05). (c) Bam8-22-induced bronchoconstriction was blocked by cholinergic blocker ipratropium bromide. (Naïve, n=6; Ipra, n=5; p=0.00085). (d) Bam8-22-induced bronchoconstriction was blocked by vagotomy. (Sham, n=7; Vagotomy, n=7; p=0.004). (e) Representative trace of airway smooth muscle contraction in response to electrical field stimulation and Bam8-22. Electrical field stimulation (12V, 8HZ, 0.5ms, 10s) induced robust contraction of mouse trachea, but Bam8-22 (10uM) did not. Arrow indicates the addition of Bam8-22. Black dots indicate the electrical field stimulation. The results were repeated in three animals.

Cholinergic contractile response of mouse trachea to electrical field stimulation (12V, 8HZ, 0.5ms, 10s) was not changed by the addition of Bam8-22 (28.3 ± 1.80 vs 30.2 ± 2.75 % of Maximum contraction). (f) Retro-orbital I.V. injection of Bam8-22 (400 μ l, 20 mg/ml) induced bronchoconstriction in guinea pigs. (PBS, n=5; Bam8-22, n=6; PBS vs Bam8-22, p=0.018). *p< 0.05, ***p< 0.005, two-tailed unpaired Student's t test. Data are reported as mean \pm s.e.m.

Author Manuscript

Author Manuscript

Author Manuscript

Author Manuscript

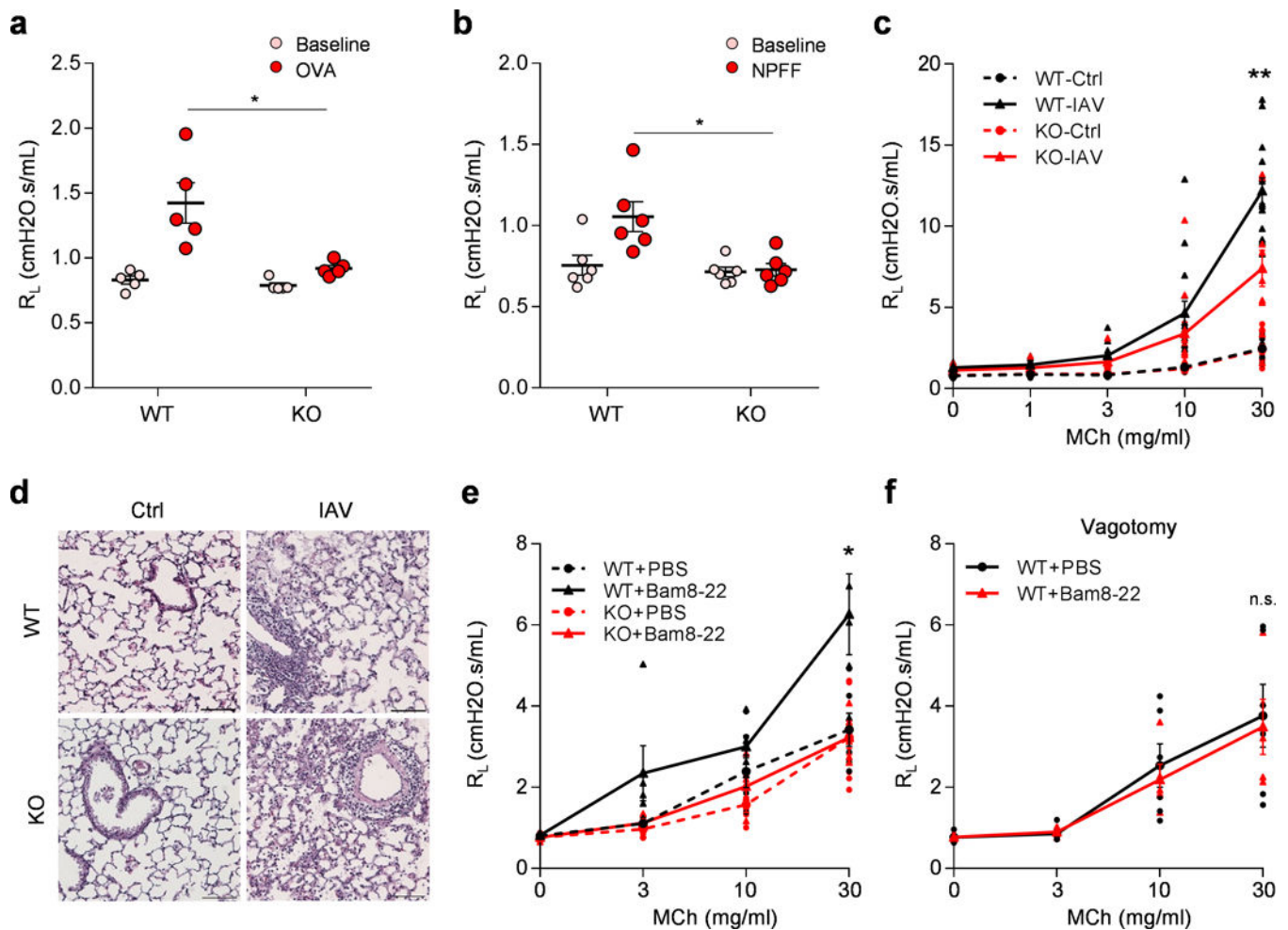


Figure 3. Mrgprs mediate anaphylactic bronchoconstriction and airway hyperresponsiveness
 (a) *Mrgpr-cluster*^{-/-} mice (n=8) exhibited attenuated anaphylactic bronchoconstriction compared to WT mice (n=6). (p=0.024). (b) Retro-orbital I.V. injection of NPFF (50 μ l, 10 mg/ml) induced bronchoconstriction in WT (n=6), but not *Mrgpr-cluster*^{-/-} mice (n=6), (p=0.014). (c) *Mrgpr-cluster*^{-/-} mice exhibited reduced airway hyperresponsiveness after influenza A virus inoculation. (WT-Ctrl, n=9; WT-IAV, n=15; KO-Ctrl, n=10; KO-IAV, n=12; WT-IAV vs KO-IAV, p=0.0051). (d) Representative H&E stained lung sections showing that wild-type and *Mrgpr-cluster*^{-/-} mice presented similar lung inflammation after influenza A virus inoculation. IFV inoculation experiment were repeated independently two times with similar results. Scale bar represents 100 μ m. (e) Bam8-22 (50 μ l, 10 mg/ml) enhanced the airway responsiveness to methacholine in wild-type, but not in *Mrgpr-cluster*^{-/-} mice. (WT+PBS, n=6; WT+Bam, n=5; KO+PBS, n=7; KO+Bam, n=5; WT+PBS vs WT+Bam, p=0.043; WT+Bam vs KO+Bam, p=0.036). (f) Vagotomy blocked Bam8-22-induced enhancement of airway responsiveness. (WT-PBS, n=6; WT-Bam, n=5; p=0.79). *p<0.05, **p<0.01, ***p<0.005, two-tailed unpaired Student's t test. Data are reported as mean \pm s.e.m.